3D Tessellation of Plant Tissue A dual optimization approach to cell-level meristem reconstruction from microscopy images

Guillaume Cerutti, Sophie Ribes, Christophe Godin, Carlos Galvan Ampudia, Teva Vernoux

3-d Tessellation of Plant Tissue
A dual optimization approach to cell-level meristem reconstruction from microscopy images

Guillaume Cerutti Sophie Ribes Christophe Godin
Virtual Plants INRIA Team
INRIA, Montpellier, France

Carlos Galvan-Ampudia Teva Vernoux
RDP, CNRS, INRA, ENS Lyon
UCBL, Université de Lyon, France

Abstract

The goal of this paper is the reconstruction of topologically accurate 3-dimensional triangular meshes representing a complex, multi-layered plant tissue structure. Based on time sequences of meristem images of the model plant Arabidopsis thaliana, displaying fluorescence markers on either cell membranes or cell nuclei under confocal laser scanning microscopy, we aim at obtaining faithful reconstructions of all the cell walls in the tissue. In the presented method, the problem is tackled under the angle of topology, and the shape of the cells is seen as the dual geometry of a 3-d simplicial complex accounting for their adjacency relationships. We present a method for optimizing such complexes using an energy minimization process, designed to make them fit to the actual adjacencies in the tissue. The resulting dual meshes constitute a light discrete representation of the cell surfaces that enables fast visualization, and quantitative analysis, and allows in silico physical and mechanical simulations on real-world data.

Keywords : *mesh optimization, voronoi diagrams, topological transformation, confocal microscopy, shoot apical meristem*

1. Introduction

The technological progresses of 3-d microscopy over the last decade have opened unprecedented perspectives for developmental biology [18] where monitoring complex growth or physiological processes at cell-level over a large amount of individuals is now made possible. However the huge amounts of produced image data require automatic or semi-automatic computational pipelines to be interpreted, and deliver quantitative information over the biological phenomena at play in the living tissue.

In the context of developmental plant biology, we focus on the shoot apical meristem (SAM), a small dome-shaped tissue formed by stem cells, located at the tip of plant stems. Every organ of the aerial part of a plant (leaves, flowers, stems...) is initiated in the SAM, which constitutes therefore the key to understanding morphogenesis (the patterning, formation and growth of the organs) and has been widely studied by plant biologists.

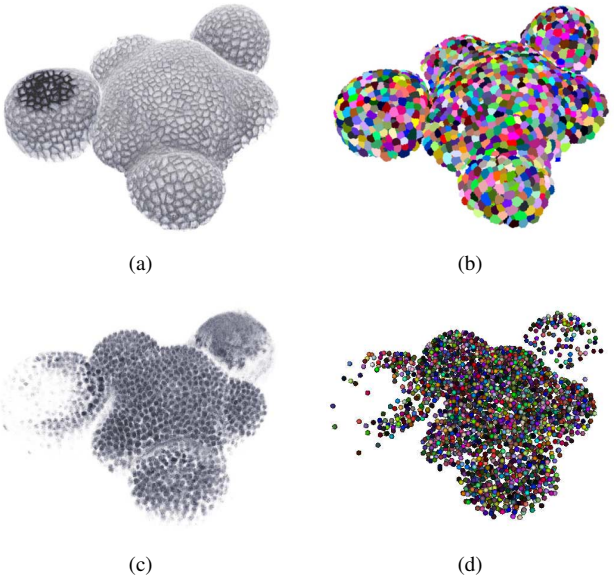

Figure 1. 3-d Confocal microscopy images of shoot apical meristems : SAM imaged with membrane marker (a) and its resulting seeded watershed segmented image [11] (b), SAM imaged with nuclei marker (c) and its resulting detected nuclei points (d)

Over the last years, an increasing number of works have proposed automatic image processing pipelines for cell reconstruction and tracking in sequences of 3-d+t microscopy SAM images (as the one displayed in Figure 1 (a)) initially focusing on the reconstruction of the surface [20] to analyze the growth and division dynamics of the first layer of cells (L1) in the meristem [1]. More recently, complete reconstructions of the dynamic multi-layered tissue structure have emerged, based on confocal laser scanning microscopy (CLSM) images, using a watershed segmentation algorithm [11] or representing cells as truncated ellipsoids [8].

A segmented image as the one presented in Figure 1 (b) is often not the most convenient object for quantitative anal-

978-1-4673-8332-5/15 $31.00 © 2015 IEEE
DOI 10.1109/3DV.2015.57

ysis, temporal registration and interpolation, or physical and biomechanical simulation. Cell walls or cell membranes surround the cells and provide all the information, from cell shapes to topological relationships, but a higher level representation of these specific objects is needed for most simulation applications [15, 4].

This explains why many computational biology works aim at reconstructing discrete topological representations of the cell boundaries, defining a triangular mesh on the surface of the meristem only [3, 2], and even in three dimensions with triangular meshes obtained from segmented images [6], or using 3-d Voronoi diagrams [25] or other forms of anisotropic tessellations on membrane images [7].

The method presented here is in line with the previously mentioned works, but focuses on the dual side of the cell shape reconstruction : their topological relationships. The Section 2 details why such an approach is pertinent in the first place. The proposed optimization method is described in Section 3 and its results evaluated in Section 4. More general conclusions are detailed in Section 5.

2. Motivation

The cell shapes in the shoot apical meristem, when we look at them in membrane image slices such as the one in Figure 2 (a), inevitably remind those of a Voronoi diagram, in their simplicity, their regularity and their arrangement. This was exploited by computational biologists, and tissue reconstruction using such a convenient tessellation has proved to be rather realistic [25, 14, 1].

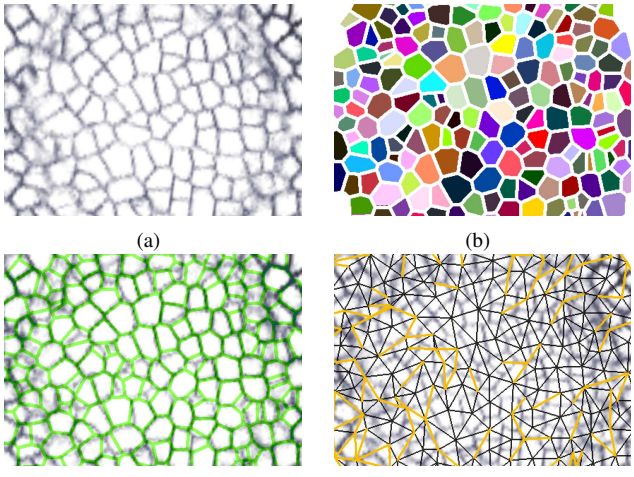

Figure 2. Reconstruction of a tissue by 2-d dual geometry : slice of a meristem imaged with membrane marker (a), its segmentation as a Voronoi diagram (b) and comparison of inexactly reconstructed cell walls (c) with false edges in the Delaunay triangulation (d)

In fact, previous works concluded that Voronoi boundaries reflect remarkably well the geometry of the cells when they are computed in 2-d (Figure 2 (c)). Topologically speaking, the Voronoi diagram is the dual of a Delaunay triangulation, where triangles correspond to points, and triangle edges to the boundaries of the Voronoi cells. And it appears that the wrong cell boundaries generally coincide with Delaunay links between cells that are not actually neighbors in the tissue, as illustrated in Figure 2 (d) (typically around 5 or 10% of the links [25]). This evidence suggests that the geometry of the cells would correspond to the dual geometry of a topological complex linking cell centers, provided the links reflect the actual relationships in the tissue.

However, when applied on 3-dimensional data, the Voronoi approach generally fails to reproduce the same convincing results [25]. The dual Delaunay complex in 3-d is composed by tetrahedra, and their edges correspond to 3-d cell interfaces. What was relatively easy in 2-d where cells were projected in a same plane, is now much more complicated due to the fact that cells are no longer co-planar and surrounded by potential neighbors in all directions.

The reconstruction problem comes with the dualization of the Delaunay complex. The points delimiting the Voronoi cells, and thus defining their geometry, are the dual of the highest dimension elements in the Delaunay complex, for instance the triangles in 2-d. An error of 5% on the links between cells (1-d elements) will result in around 20% of error on the triangles, and on the corresponding dual cell points. But in 3-d, we observed a typical 25% of error on cell links, that results in nearly 80% error on the tetrahedra of the Delaunay simplicial complex, making a plausible reconstruction of cell shapes very unlikely.

Plant cell tissue does not constitute a proper Voronoi diagram, but it still forms a cell complex, dual of an adjacency complex [1]. The reason why Voronoi cells are not satisfying is the strong, locally varying, anisotropy of the cell shapes resulting from individual growth and division processes. The use of other tessellation methods such as power diagrams or Centroidal Voronoi Tessellations (CVT) [9] would introduce too much regularity for this biological reality.

On the other hand, it has been shown that other anisotropic tessellations were perfectly able to reconstruct adequate cells, with a faithful shape [7] based on a precise estimation of this anisotropy. Anisotropic Voronoi diagrams [21] or anisotropic CVT [22] assume that a smooth anisotropy field is known. However these assumptions are not compatible with plant tissue where cell principal directions may vary importantly between neighbors [26].

We propose a method based on the adjacency relationships of the cells in the tissue, which actually constitute a manifestation of the local anisotropy. The reconstruction of the tissue images is performed by the dualization of a topological complex that reflects those relationships better than the Delaunay complex, capturing this essential biological anisotropy information. The outline of the method is given in Figure 3.

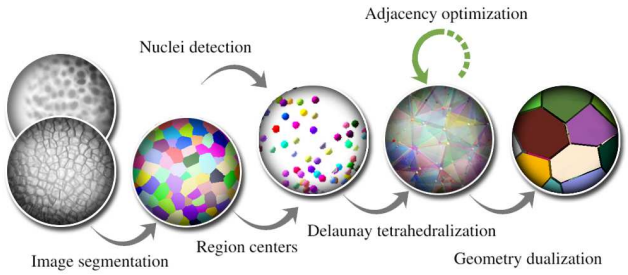

Figure 3. Summary of the reconstruction process

3. Adjacency optimization

The main goal of the method is to represent faithfully the topology of the tissue, namely the neighborhood relationships between cells, seen as the vertices of a topological complex. It supposes that those cells have been detected beforehand and their spatial position is known, typically after a 3-d watershed segmentation of a confocal image displaying membrane markers [11] where cells are identified and their position set as the barycenter of their region. But it is also possible to work on images showing nuclei markers (Figure 1 (c)), in which cells can be detected using common approaches of blob detection, such as scale-space maxima of difference of Gaussians (DoG) [23] (Figure 1 (d)).

In the case of segmented images, a substantial information on adjacency is available, as two neighbor voxels with different labels indicate a link between neighbor cells. However this topology information is sensitive to the discretization of data, to noise in the signal and to segmentation errors. Though some corrections might be done to enhance the adjacency graph (removal of links when the interface surface is small for instance) it will generally not be possible to build a valid simplicial complex out of it. As for detected nuclei, there is no information at all concerning the neighbors of a given cell, and only the relative position of points might help.

In any case, the Delaunay tetrahedralization of the cell points provides a first approximation of the adjacency relationships that has the advantage of being a well-defined simplicial complex, making deformation operations and dualization much more convenient.

3.1. Adjacency as a simplicial complex

In the following, we represent the adjacency between cells by a simplicial complex of dimension 3, in other terms a tetrahedral mesh whose vertices are the points corresponding to the identified cells in the tissue. The simplicial definition makes a strong assumption: since the dimension 3 elements are tetrahedra, no more than 4 cells can be simultaneously adjacent (or, there can not be any 5-clique in the cell adjacency graph). This hypothesis is consistent with what can be observed in tissue images, where no more than 4 cells (or 3 at the surface) meet at a given point, and is therefore very important to preserve the biological plausibility of the tissue we are reconstructing.

A tetrahedral mesh $\mathcal{T}$ is defined as a 3-d incidence graph, composed of:

- 4 sets of elements $(\mathcal{W}_0, \mathcal{W}_1, \mathcal{W}_2, \mathcal{W}_3)$ accounting respectively for vertices, edges, triangles and tetrahedra
- 3 topological boundary relationships $(\mathcal{B}_1, \mathcal{B}_2, \mathcal{B}_3)$ delimiting the elements of dimensions 1, 2 and 3 by their boundaries in the lower dimension
- A geometrical information $\{\mathcal{P}(c), c \in \mathcal{W}_0\}$ determining the positions of the vertices (here the cell centers)

In this case, the number of boundaries for an element of dimension d will always be equal to $d+1$ given the simplicial constraint. For instance any triangle $t \in \mathcal{W}_2$ will have $\mathcal{B}_2(t) = (e_1, e_2, e_3)$ with $e_1, e_2, e_3 \in \mathcal{W}_1$.

The boundary relationship $\mathcal{B}_d$ defines a converse region relationship $\mathcal{R}_{d-1}$ listing, for an element, all the elements of greater dimension for which it constitutes a boundary: $\forall w \in \mathcal{W}_d, \mathcal{R}_d(w) = \{w' \in \mathcal{W}_{d+1} \mid w \in \mathcal{B}_{d+1}(w')\}$. The notion of boundaries (and regions) can be extended to other dimensions by mere transitivity, and noted $\mathcal{B}_d^n$ with $\mathcal{B}_d^1$=$\mathcal{B}_d$: $\forall w \in \mathcal{W}_d, \mathcal{B}_d^n(w) = \bigcup_{u \in \mathcal{B}_d(w)} \mathcal{B}_{d-1}^{n-1}(u)$. This also defines two different neighborhood relationships between elements of the same dimension d : $\mathcal{N}_d^-$ listing the elements that share a boundary with a given element, and the converse $\mathcal{N}_d^+$ listing the elements that share a region with it.

With this formulation, the input data consists of $\mathcal{W}_0$ and $\mathcal{P}$, the identified cells and the positions of their center point in space. Based on this, the Delaunay tetrahedralization provides an initial tetrahedral mesh $\mathcal{T}_\Delta = \left(\mathcal{W}_0, \mathcal{P}, \mathcal{W}_1^\Delta, \mathcal{B}_1^\Delta, \mathcal{W}_2^\Delta, \mathcal{B}_2^\Delta, \mathcal{W}_3^\Delta, \mathcal{B}_3^\Delta\right)$ similar to the one displayed in Figure 4 (a). The optimization problem consists then in finding the solution $\left(\mathcal{W}_1, \mathcal{B}_1, \mathcal{W}_2, \mathcal{B}_2, \mathcal{W}_3, \mathcal{B}_3\right)$ that best approximates the adjacencies between cells in the tissue.

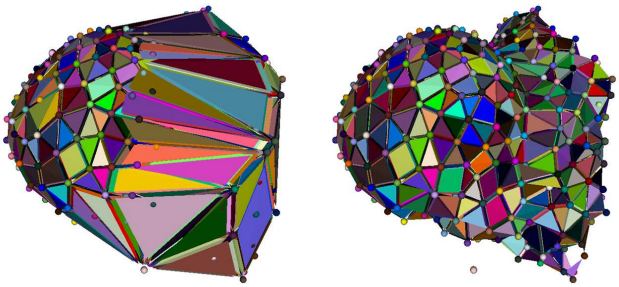
(a) (b)

Figure 4. Delaunay tetrahedralization of cell points detected in the image of a developing flower in the SAM (a) and its optimized version after cleaning of oversized triangles (b)

3.2. Tetrahedral mesh optimization

The mesh optimization we consider is somewhat particular in the sense that it can not affect the mesh geometry $\mathcal{P}$, and therefore will not incorporate any smoothing which is

often used to improve the quality of a mesh [12, 13]. Neither is it possible to insert or remove vertices that would ameliorate the mesh elements [5, 27, 19] since the set of cells defining the vertices $\mathcal{W}_0$ is fixed.

Consequently, the only possible deformations of the mesh consist in topological operations, reconfiguring locally the connections between vertices and the mesh elements of higher dimension. Various topological transformation are possible, but almost all of them require a specific configuration of the tetrahedra to ensure that the operation does not alter the validity of the mesh (loss of simplicial criterion, intersection of elements). The described possible topological transformations are the following:

- **Triangle swapping** (or **2-3 flip**) [13] : consisting in transforming any interior triangle separating 2 tetrahedra into an edge between their opposite vertices, creating 3 new tetrahedra (Figure 5 (a))
- **3-2 flip** : the reverse operation, converting an edge with 3 incident tetrahedra into the triangle linking their 3 other vertices (Figure 5 (a))
- **4-4 flip** : consisting in transforming an edge with 4 incident tetrahedra into another edge linking 2 opposite vertices among their 4 other vertices, creating 4 new tetrahedra
- **Edge removal** [5, 19, 28] : converting any edge with n incident tetrahedra into a triangulation of all their other vertices, creating $2n - 4$ new tetrahedra, an operation that generalizes the 3-2 flips and 4-4 flips (Figure 5 (b))
- **Multi-face removal** [19, 28] : the reverse operation, converting any set of triangles sandwiched between the two same vertices into the edge between those vertices, an operation that generalizes 2-3 flips, as well a some cases of 4-4 flips (Figure 5 (b))
- **Multi-face retriangulation** [24] : consisting in transforming any set of triangles sandwiched between the two same vertices into a new triangulation of all their vertices, creating the same number of tetrahedra

Among these, we retained only two operations: **triangle swapping** and **edge removal**, that share the advantage of being directly based on the elements of a simplicial complex, respectively of dimension 1 and 2 regardless of their topological configuration (the geometrical applicability still needs to be checked to ensure no intersection is created). The interest of multi-face removal appeared limited, since the most common configuration (apart from 2-3 flips) is a 4-4 flip configuration that might as well be handled by edge removal. The computational complexity of the multi-face retriangulation, made us prefer more basic transformation that, combined, might generally produce the same result.

Concerning the edge removal transformation, we made the operation unique not by selecting the best triangulation of the neighboring vertices of an edge, but by considering only the Delaunay triangulation of their projections on the median plane of the edge. Given that, in 2 dimensions, Delaunay provides a satisfactory approximation of the cell adjacencies, we made the hypothesis that this triangulation would generally be the right choice, plus making all the topological tranformations we consider unequivocal.

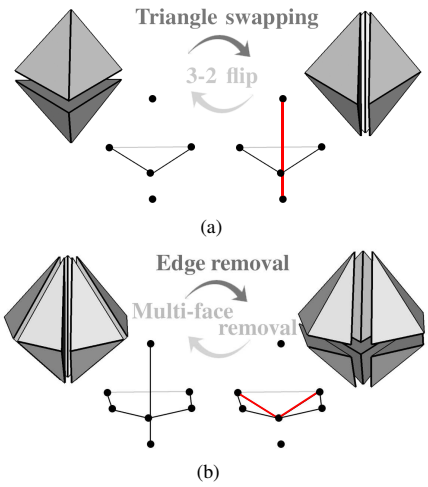

Figure 5. Topological transformations on a tetrahedral mesh : triangle swapping operation (a) and edge removal operation (b)

3.3. The exterior trick

The problem with the simplicial complex and the operations defined as such is that they do not make it possible to transform the topology at the exterior border of the complex. Exterior triangles belong to a single tetrahedron and therefore can not be swapped, and exterior edges might have only 2 neighboring vertices, which can not be triangulated in edge removal. Modifying the adjacencies between cells at the surface of the tissue is nevertheless crucial to obtain a plausible reconstructed volume.

To solve this problem, we introduced an artificial exterior vertex v_{ext} representing a hypothetical "exterior cell". We complete the Delaunay simplicial complex $\mathcal{T}_\Delta$ by adding new exterior tetrahedra: for each exterior triangle $t \in \mathcal{W}_2^\Delta$ such that $|\mathcal{R}_2^\Delta(t)| = 1$ we add a new tetrahedron which vertices are those of t plus v_{ext}. With this definition, the topological operations will produce changes at the surface, in particular 4-4 flips produced by edge removal when v_{ext} is a neighbor vertex will produce the same effect on the surface that a 2-d edge flip on a triangular surface mesh.

The tricky part comes from the fact that the exterior does not have a unique geometrical position as the rest of the vertices do, and its position will have strong impacts to determine if a configuration allows for a topological transformation, or if an operation is applicable or not. Therefore, we are forced to determine for each element of the mesh where its relative exterior lies. We approximate these relative positions using the normal vectors at the vertices of the mesh, always oriented towards its exterior, and placing

the exterior at a typical distance from the barycenters of the edges or triangles following their mean normal vector.

The first operation performed on this newly defined simplicial complex $\mathcal{T}_{\Delta'}$ consists in removing aberrant elements. A seen in Figure 4 (a) one issue with the Delaunay tetrahedralization is that it produces a convex topological complex, when the underlying structure most often present large concave parts. It is therefore necessary to remove the false exterior triangles that come covering these concave parts, which are generally oversized.

This is done by iteratively performing passes of **triangle swapping** operations on triangles separating v_{ext} and another vertex. The swapping of the triangle (Figure 5 (a)) basically removes it from the surface of the triangulation, as it creates 3 new tetrahedra joining the 3 other faces of the original interior tetrahedron and the exterior. The decision of swapping or not a triangle is made following a threshold criterion: if the maximal length of an edge of the triangle exceeds l_{max}, the triangle is swapped.

This first optimization results in a simplicial complex noted $\mathcal{T}_{\Delta\star}$ that constitutes a much more plausible approximation of the tissue topology (Figure 4 (b)) that still respects the Delaunay criterion. It is similar to what would produce an α-shape [10] of value $\alpha = l_{max}$, with the notable difference that by using such a topological optimization, we guarantee that it contains only tetrahedra and no hole inside the tissue (a strong biological prior).

3.4. Energy minimization

Starting from $\mathcal{T}_{\Delta\star}$, our goal is to optimize the connectivity of the adjacency simplicial complex $\mathcal{T}$ using the introduced local topological transformations to reproduce the ones in the tissue here represented by its segmented image $\mathcal{S}$, in the case of a membrane marker image. We chose to formulate this optimization as an energy minimization problem, a common approach for mesh optimization [16]. Following the widespread formalism regarding deformable models, from their first application to contour detection [17], the energy functional we aim at minimizing is decomposed into an external data attachment term, a shape prior term and an internal regularization term:

$$E(\mathcal{T},\mathcal{S}) = E_{image}(\mathcal{T},\mathcal{S}) + E_{prior}(\mathcal{T}) + E_{regularity}(\mathcal{T}) \tag{1}$$

In our case the image attachment energy has the role of making the adjacency complex fit with the relationships between cells that can be found in the case of a segmented cell image $\mathcal{S}$. Screening through the image, it is possible to detect the voxels around which at least 4 different labels can be found. They correspond to cell corners, and their detection creates a set of 4-uples $T_{\mathcal{S}} = \{(v_1, v_2, v_3, v_4)\}$ of cell labels that match the vertices of $\mathcal{T}$ (including v_{ext} that matches the label used for the exterior region in the image). It is important to note that, even though $T_{\mathcal{S}}$ could be seen as a set of tetrahedra, its topological properties does not make it a valid simplicial complex, and its dualization would not result in a consistent reconstruction of the tissue.

We use $T_{\mathcal{S}}$ as a set of reference tetrahedra to which the tetrahedra of $\mathcal{T}$ should fit as well as possible. Consequently, the data attachment energy term we use simply measures the overlap between $T_{\mathcal{S}}$ and the tetrahedra of the current simplicial complex $T_{\mathcal{T}} = \{\mathcal{B}_3^3(t), t \in \mathcal{W}_3\}$, computed as a Jaccard index that we want to maximize:

$$E_{image}(\mathcal{T},\mathcal{S}) = -\omega_{adjacency}\frac{|T_{\mathcal{T}} \cap T_{\mathcal{S}}|}{|T_{\mathcal{T}} \cup T_{\mathcal{S}|}} \tag{2}$$

The prior energy term is here to incorporate some exterior knowledge in the optimization process, and in our context give more biological plausibility to the result. For a plant tissue, an important constraint is the number of neighbors one cell can have, that follows a regular distribution throughout the tissue. By studying neighborhood relationships in segmented tissue images, we remarked that the number of neighbors of an epidermis cell was 9.0 ± 2.1 and 13.0 ± 2.7 for an inner cell. Consequently, we set $N_{epi} = 9$ and $N_{inn} = 13$ and define the prior energy using the distance of the number of neighbors of each vertex to its ideal value (depending whether it touches the exterior or not):

$$E_{prior}(\mathcal{T}) = \omega_{neighbor}\frac{1}{|\mathcal{W}_0|}\sum_{v\in\mathcal{W}_0\setminus v_{ext}}\left(|\mathcal{N}_0^+(v)| - N(v)\right)^2 \tag{3}$$

$$\forall v \in \mathcal{W}_0 \setminus v_{ext}, N(v) = \begin{cases} N_{epi}+1 & \text{if } v_{ext} \in \mathcal{N}_0^+(v) \\ N_{inn} & \text{otherwise} \end{cases}$$

And finally, the inner energy term aims at adding a regularization constraint to the geometry of the mesh elements. It tries to improve the quality of the tetrahedra in a way that should fit the goal of recreating a plausible cell adjacency. With this goal, we defined it on the tetrahedra of $\mathcal{T}$, trying to avoid that links appear between cells that are too distant by measuring the maximal edge length of each tetrahedron:

$$E_{regularity}(\mathcal{T}) = \omega_{length}\frac{1}{|\mathcal{W}_3|}\sum_{t\in\mathcal{W}_3}\max_{\substack{e\in\mathcal{B}_3^2(t)\\(v_1,v_2)=\mathcal{B}_1(e)}}\|\mathcal{P}(v_1) - \mathcal{P}(v_2)\| \tag{4}$$

The sum of these energies is then minimized following an iterative, annealing-like, optimization process, a succession of temperature cycles divided in two phases of topological transformations: one consisting in edge removals, and the second one in triangle swaps. In each phase, the tetrahedra resulting from the transformation of each edge and each triangle respectively are computed, and the local energy variations associated with the modification of the tetrahedra impacted by the transformations estimated. The edges (resp. triangles) are ranked in ascending order of the energy variation, and the legal operations are performed

in that order, with a temperature-dependent probability for transformations leading to an increase of the energy.

The termination criterion was set as a number of iterations, and our experiments concluded that 5 temperature cycles were enough to optimize the complex. The energy having different, sometimes antagonist effects, it is important to balance well their influence to get the best result. The values $\omega_{adjacency} = 8.0$, $\omega_{neighbor} = 0.05$ and $\omega_{length} = 0.5$ empirically proved to offer the best compromise.

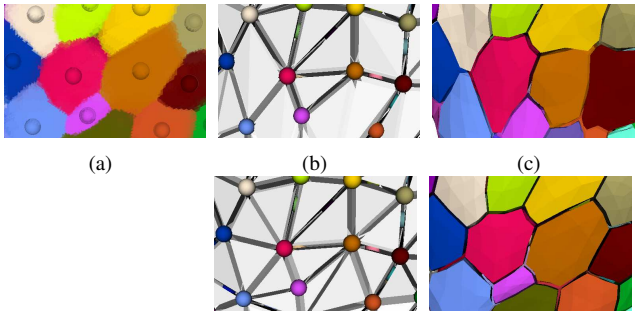

(a) (b) (c) (d) (e)

Figure 6. Reconstruction of plant tissue through adjacency optimization: segmented tissue image with located cell points (a), cleaned-up Delaunay tetrahedralization of the cells (b) and triangular mesh obtained from the dual Voronoi diagram (c), and result of the optimization of the adjacency simplical complex (d) with the more accurate reconstructed dual geometry of the tissue (e)

4. Results and opened perspectives

We performed tests over two different sets of images: images of membrane marker of floral meristems segmented using the MARS pipeline [11] with segmented region centers used as cell points, and images of nuclei marker of shoot apical meristems with nuclei points detected as scale-space maxima of DoG. In the first case, the optimization was based on image data and the complete energy could be used, as well as the image adjacencies for evaluation of the results. The second case was performed to assess the results without any information on adjacency, and only prior and regularity energy terms could be used. Tests were performed following this constraint on images from the first set to try to evaluate the accuracy of the approach.

4.1. Optimization results

The energy minimization process produces an optimal mesh $\mathcal{T}^\star$ (Figure 6 (c)) that is significantly different from the initial one $\mathcal{T}_{\Delta\star}$ (Figure 6 (b)). To evaluate the quality of this adjacency simplicial complex, the most significant indicator is the comparison between the adjacency relationships in the mesh and in the segmented image $\mathcal{S}$. This can actually be performed in several different ways, depending on the number of cells used to define an adjacency:

- Considering cells 2 by 2 (**2-adjacency**) we can compare edges of the adjacency complex $E_\mathcal{T} = \{\mathcal{B}_1(e), e \in \mathcal{W}_1\}$ with the set of all pair of cells sharing an interface (large enough) in the segmented image, noted $E_\mathcal{S}$.
- Considering cells 4 by 4 (**4-adjacency**) we can compare directly the tetrahedra of the adjacency complex $T_\mathcal{T}$ with the 4-uples reprensenting the junction points of 4 cells in the image $T_\mathcal{S}$.

Both criteria are computed as Jaccard indexes between the two compared sets, with values ranging from 0 for no overlap to 1 only when the overlap is perfect. The second criterion is of course more constraining, but it is a better indication on the quality of the result: since the cell corners, dual of the adjacency tetrahedra, define the geometry of the cell, their adequation to the image really reflects how well we may reconstruct the tissue. The simple cell adjacency measure is also important to have an idea of which proportion of the reconstructed interfaces actually exists in the tissue.

In addition to these topological values, we also measure other estimators of quality, to observe their correlation with these target indicators, and assess the relevance of their optimization in the case that no information on adjacency is available (as in the case of nuclei marker images). We use the average **neighborhood error**, computed as in Equation 3 to measure the regularity of cell neighborhood. The intrinsic quality of the mesh is measured using common measures such as the average **tetrahedra eccentricity** (computed using shape factor), and the average **minimal** and **maximal dihedral angles** of the tetrahedra triangle planes.

We computed those measures over a dozen of segmented meristem images with a typical number of cells varying between 800 and 2000. They were computed for the three steps of the optimization method: the Delaunay tetrahedralization $\mathcal{T}_\Delta$, its version after the oversized triangle swapping phase $\mathcal{T}_{\Delta\star}$, and its optimized version $\mathcal{T}^\star$. The evaluation measures averaged over the dataset are given in Table 1.

Table 1. Evaluation of the adjacency optimization over a set of segmented meristem images

	2-adj	4-adj	N error	T ecc	min angle	max angle
$\mathcal{T}_\Delta$	0.68	0.28	0.12	0.45	37.4	117.5
$\mathcal{T}_{\Delta\star}$	0.76	**0.33**	0.11	0.42	39.2	116.5
$\mathcal{T}^\star$	0.89	**0.76**	0.10	0.39	39.7	116.1

The main observation that can be drawn from these results is the significant improvement that is achieved regarding cell adjacency relationships, jumping from an average Jaccard score of 0.33 to 0.76 through topological optimization. This means that, even if the links between 2 cells show a 0.76 overlap, the Delaunay tetrahedralization is overall wrong concerning cell corners, and the method we propose manages to covert it into an overall more consistent simplicial complex. The consequence is that many more points will be correct when reconstructing the tissue, producing a much more accurate representation.

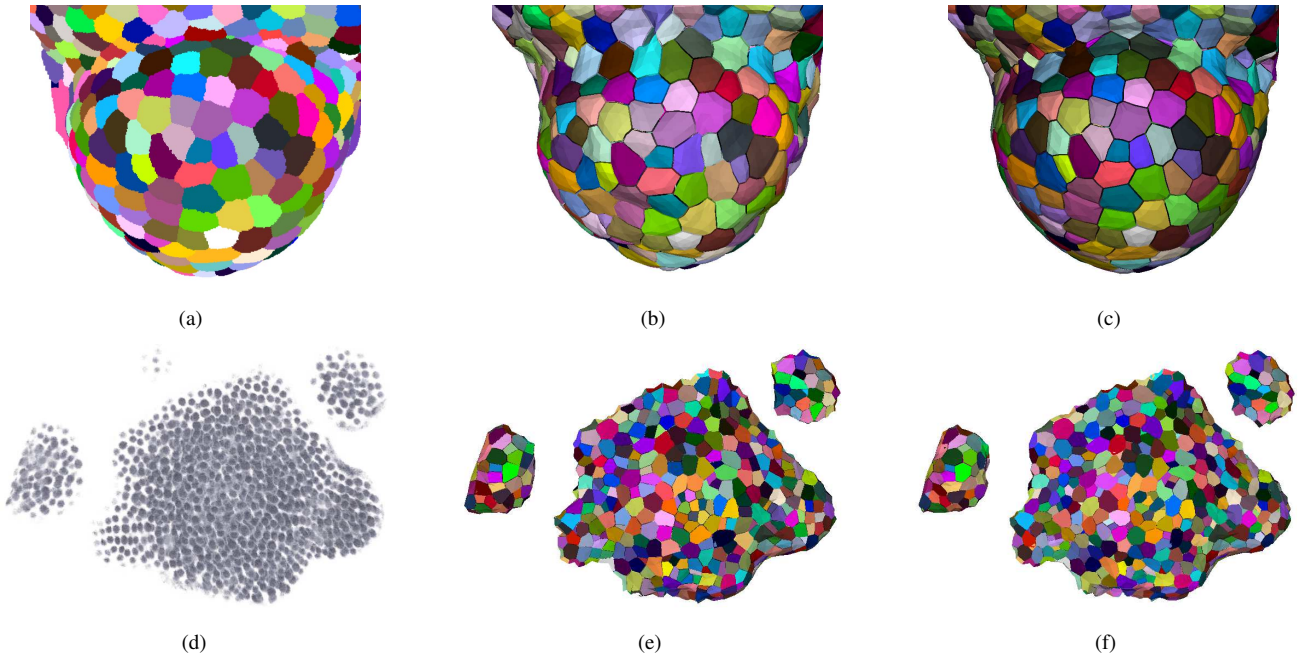

Figure 7. Tessellation for tissue reconstruction : floral mersitem imaged with membrane marker and segmented (a) and shoot apical meristem imaged with nuclei marker (d); dual geometry obtained from Delaunay tetrahedralization (b)-(e) and reconstructed tissue mesh after adjacency optimization (c)-(f)

The other interesting fact is that the other quality estimators seem correlated to the improvement of the adjacency, in the good direction (decrease of the neighborhood error and increase of the tetrahedra regularity). The improvement is weak though, and there is not a very clear sign that trying to improve those factors only will end up producing a great correction of the adjacency, though it would contribute to it in a moderate extent.

4.2. Segmented tissue reconstruction

To produce an actual reconstruction of the cells in the tissue, the missing step is to build the dual geometry of the simplicial complex $\mathcal{T}^\star$. Topologically speaking, it can be seen as an inversion of the dimensionality of its elements, and of the boundary and region relationships $\mathcal{B}$ and $\mathcal{R}$, resulting in a dual mesh $\mathcal{G} = \big(\mathcal{D}_0, P, \mathcal{D}_1, \mathcal{B}_1, \mathcal{D}_2, \mathcal{B}_2, \mathcal{D}_3, \mathcal{B}_3\big)$. For instance the edges in $\mathcal{W}_1$ will generate faces in the dual geometry, and the borders $\mathcal{B}_2(f)$ of the dual face f corresponding to the edge e will be the dual edges corresponding to the triangles $\mathcal{R}_1(e)$ incident on e.

The geometry of the whole mesh is once again determined only by the positions of the elements of dimension 0, here cell corners. In the dualization process, the dual vertices in $\mathcal{D}_0$ corresponding to tetrahedra in $\mathcal{W}_3$, the position of ν corresponding to a tetrahedron T has to be computed using the position $\mathcal{P}$ of the 4 vertices $\mathcal{B}_3^3(T)$ of T using a geometrical transform function g. The creation of the dual geometry consists then in building a mesh $\mathcal{G}$ such that:

- $\mathcal{D}_0 = \{\nu | \nu = T \in \mathcal{W}_3\}$
- $\forall \nu \in \mathcal{D}_0, P(\nu) = g(\{\mathcal{P}\big(\mathcal{B}_3^3(T)\big) \mid \nu = T \in \mathcal{W}_3\})$
- $\mathcal{D}_1 = \{\epsilon | \epsilon = t \in \mathcal{W}_2\}$
- $\forall \epsilon \in \mathcal{D}_1, \mathcal{B}_1(\epsilon) = \{\nu \mid \nu = T \in \mathcal{R}_2(t), \epsilon = t \in \mathcal{W}_2\}$
- $\mathcal{D}_2 = \{f | f = e \in \mathcal{W}_1\}$
- $\forall f \in \mathcal{D}_2, \mathcal{B}_2(f) = \{\epsilon \mid \epsilon = t \in \mathcal{R}_1(e), e = f \in \mathcal{W}_1\}$
- $\mathcal{D}_3 = \{c | c = v \in \mathcal{W}_0\}$
- $\forall c \in \mathcal{D}_3, \mathcal{B}_3(c) = \{f \mid f = e \in \mathcal{R}_0(v), c = v \in \mathcal{W}_0\}$

To match the shapes produced by a Voronoi diagram, that proved to convey some realism, we defined the geometrical function g so that it places the dual point of a tetrahedron at the center of the circumsphere of its vertices. However, to ensure the validity of the reconstructed geometry, it seemed safer that all the points remained inside their respective tetrahedron to avoid intersections and folding. Consequently, if the center of a circumsphere lies outside its tetrahedron, it is projected to the center of the circumcircle of the closest triangle, and if it lies again outside this triangle, it is projected to the middle of the closest edge.

Concerning tetrahedra containing v_{ext} as one of their vertices, it has been chosen to consider simply the center of the circumcircle of the triangle without v_{ext}, rather than trying to estimate a realistic exterior position. This generates a slight lowering of the tissue surface, that can be corrected afterwards. The geometry defined this way, as displayed in Figure 7 (c), conforms with a Voronoi diagram in the regular cases, while ensuring that no problematic configurations will arise in the dualization process.

The cell interfaces in $\mathcal{G}$ are defined by a set of edges that do not necessarily define a planar polygon, even less a triangle. To make visualization, computation and all other applications possible on the object, it is necessary to produce a triangular interface mesh out of it. There are different ways to convert the interfaces of $\mathcal{D}_2$ into a set of triangles suitable for the desired application (Delaunay triangulation again, fitting of a regular triangular grid of chosen fineness) and we chose a star-shaped triangulation of the polygon by adding a vertex corresponding to its barycenter, and linking all the edges to it. This is followed by the 4-split of all triangles, and by a smoothing phase optimizing the shape of the triangles [29, 6].

The reconstructed tissue presents very interesting traits compared with triangular meshes with similar complexity that can be generated directly from the voxel image, using tetrahedral mesh generation [27] for instance. For a similar number of mesh elements, on the same images, those directly generated meshes might show a better 2-adjacency Jaccard index (**0.91** vs. **0.89**) but the index for 4-adjacency is significantly lower (**0.69** vs. **0.76**). This means that if the interfaces are well identified by direct meshing techniques, they will be topologically better represented by the dual approach we presented.

More importantly, those meshes produce a significant proportion of vertices where more than 4 cells coincide, which may be a major problem for biologically accurate simulations. Among all the cell corners in those meshes we detect an average of **12%** of them showing such a problematic configuration, when our method structurally creates **none**. This makes the tissue we reconstruct a better tool for growth simulations, or other finite element based biomechanical of biophysical applications, provided the quality of the triangles is sufficiently improved by the smoothing.

4.3. Reconstruction from nuclei

In the case of cells detected from nuclei markers, the cleaned-up Delaunay complex $\mathcal{T}_{\Delta\star}$ is optimized using only the prior and regularization energy terms, with no data attachment since there is no adjacency data to rely on. It is therefore very difficult to assess to which extent the optimized topology $\mathcal{T}^\star$ is more accurate than the original one and how much improved the cell geometry is, except from the angle of regularity and visual plausibility.

The closest to a quantitative analysis we can do is to simulate nuclei detection by centers of segmented regions in membrane images, knowing that the position of the nucleus does not necessarily coincide with the center of the cell. For a better evaluation, we would need meristems imaged with both membrane and nuclei markers, which is biologically and technically difficult. Still we evaluated the topology optimization based on those energies on the same images as previously, with the results presented in Table 2.

Table 2. Evaluation of the adjacency optimization with no data attachment energy over a set of segmented meristem images

	2-adj	**4-adj**	**N error**	**T ecc**	**min angle**	**max angle**
$\mathcal{T}_\Delta$	0.68	0.28	0.12	0.45	37.4	117.5
$\mathcal{T}_{\Delta\star}$	0.76	0.33	**0.11**	**0.42**	**39.2**	116.5
$\mathcal{T}^\star$	0.73	0.29	**0.07**	**0.31**	**44.7**	116.1

The result is that no sensible improvement of the topological relationships seemed to be achieved by the optimization, though the produced complex presents a more regular stucture and gives a more realistic tissue as shown in Figure 7 (f). This is to balance by the fact that cell centers are not nuclei, but it would appear that geometry itself is not decisive enough to help guess adjacencies between cells in a complex multi-layered tissue, as indicates the performance observed on the 3-d Voronoi diagrams. Still the method produces a plausible tissue structure with interesting topological properties, that could make it handy for simulations when only nuclei data is available.

5. Conclusions

The tissue reconstruction method we described constitutes a new step bridging the gap between imaged experimental data and higher-level computational simulations. Based on a tissue imaged with a membrane marker, it produces, after segmentation, a topologically accurate representation of the tissue as a triangular mesh of adaptable complexity. Its inherent topological properties (adequation with the adjacency relationships in the tissue, respect of biological constraints regarding cell intersection) along with its good quality triangles in a compact structure makes it ideal for biophysical simulations.

The method offers the possibility of creating a continuous 3-d tissue structure from discrete data points, while ensuring desirable properties, a novelty in the case of meristems imaged with nuclei markers. The produced structure is a helpful tool for fast computation of volumes, principal curvatures or other shape statistics that are useful to monitor throughout time in the context of plant morphogenesis. It constitutes also a good way to visualize the tissue and to project functional information on cells (such as expression of genetic markers allowing to trace morphogenetic signals distribution or cell identities) in a continuous way on a whole volume.

Finally, the angle of topology is critical when it comes to reconstructing 4-d plant tissue as an interpolation of consecutive images of an individual at different time points. Provided we are able to compute the cell lineage, the interpolation of the simplicial complex of adjacency would be a rather straightforward process, making the generation of an interpolated dual geometry almost implicit. Such a 4-d object preserving the properties of the tissue would be of great interest for spatio-temporal registration of meristem image sequences, and a major step towards the constitution of a 4-d atlas of complex dynamic tissues such as the meristem.

References

[1] P. Barbier de Reuille, I. Bohn-Courseau, C. Godin, and J. Traas. A protocol to analyse cellular dynamics during plant development. *The Plant Journal*, 44(6):1045–1053, 2005.

[2] P. Barbier de Reuille, S. Robinson, and R. S. Smith. Quantifying cell shape and gene expression in the shoot apical meristem using MorphoGraphX. In *Plant Cell Morphogenesis*, pages 121–134. 2014.

[3] P. Barbier de Reuille, A.-L. Routier-Kierzkowska, D. Kierzkowski, G. W. Bassel, T. Schüpbach, G. Tauriello, N. Bajpai, S. Strauss, A. Weber, A. Kiss, A. Burian, H. Hofhuis, A. Sapala, M. Lipowczan, M. B. Heimlicher, S. Robinson, E. M. Bayer, K. Basler, P. Koumoutsakos, A. H. Roeder, T. Aegerter-Wilmsen, N. Nakayama, M. Tsiantis, A. Hay, D. Kwiatkowska, I. Xenarios, C. Kuhlemeier, and R. S. Smith. MorphoGraphX: A platform for quantifying morphogenesis in 4d. *eLife*, 4, 2015.

[4] F. Boudon, J. Chopard, O. Ali, B. Gilles, O. Hamant, A. Boudaoud, J. Traas, and C. Godin. A Computational Framework for 3D Mechanical Modeling of Plant Morphogenesis with Cellular Resolution. *PLoS Computational Biology*, 11(1):1–16, 2015.

[5] E. Brière de Lisle and P.-L. George. Optimization of tetrahedral meshes. In *Modeling, Mesh Generation, and Adaptive Numerical Methods for PDEs*, volume 75 of *The IMA Volumes in Mathematics and its Applications*, pages 97–127. Springer New York, 1995.

[6] G. Cerutti and C. Godin. Meshing meristems - an iterative mesh optimization method for modeling plant tissue at cell resolution. In *BIOIMAGING*, 2015.

[7] A. Chakraborty, M. M. Perales, G. V. Reddy, and A. K. Roy Chowdhury. Adaptive geometric tessellation for 3d reconstruction of anisotropically developing cells in multilayer tissues from sparse volumetric microscopy images. *PLoS One*, 8(8), 2013.

[8] A. Chakraborty, R. Yadav, G. V. Reddy, and A. K. Roy Chowdhury. Cell resolution 3d reconstruction of developing multilayer tissues from sparsely sampled volumetric microscopy images. In *BIBM*, pages 378–383, 2011.

[9] Q. Du, V. Faber, and M. Gunzburger. Centroidal voronoi tessellations: Applications and algorithms. *SIAM Rev*, pages 637–676, 1999.

[10] H. Edelsbrunner and E. P. Mcke. Three-dimensional alpha shapes, 1994.

[11] R. Fernandez, P. Das, V. Mirabet, E. Moscardi, J. Traas, J.-L. Verdeil, G. Malandain, and C. Godin. Imaging plant growth in 4D : robust tissue reconstruction and lineaging at cell resolution. *Nature Methods*, 7:547–553, 2010.

[12] D. A. Field. Laplacian smoothing and delaunay triangulations. *Communications in Applied Numerical Methods*, 4(6):709–712, 1988.

[13] L. A. Freitag and C. Ollivier-Gooch. Tetrahedral mesh improvement using swapping and smoothing. *International Journal for Numerical Methods in Engineering*, 40(21):3979–4002, 1997.

[14] V. Gor, B. Shapiro, H. Jönsson, M. Heisler, G. Reddy, E. Meyerowitz, and E. Mjolsness. A software architecture for developmental modeling in plants: The computable plant project. In N. Kolchanov, R. Hofestaedt, and L. Milanesi, editors, *Bioinformatics of Genome Regulation and Structure II*, pages 345–354. Springer US, 2006.

[15] O. Hamant, M. G. Heisler, H. Jönsson, P. Krupinski, M. Uyttewaal, P. Bokov, F. Corson, P. Sahlin, A. Boudaoud, E. M. Meyerowitz, Y. Couder, and J. Traas. Developmental patterning by mechanical signals in arabidopsis. *Science*, 322:1650–1655, 2008.

[16] H. Hoppe, T. DeRose, T. Duchamp, J. McDonald, and W. Stuetzle. Mesh optimization. In *Proceedings of the 20th Annual Conference on Computer Graphics and Interactive Techniques*, SIGGRAPH '93, pages 19–26, 1993.

[17] M. Kass, A. Witkin, and D. Terzopoulos. Snakes: Active contour models. *International Journal of Computer Vision*, 1(4):321–331, 1988.

[18] P. J. Keller. Imaging morphogenesis: Technological advances and biological insights. *Science*, 340(6137), 2013.

[19] B. M. Klingner and J. R. Shewchuk. Aggressive tetrahedral mesh improvement. In *Proceedings of the 16th International Meshing Roundtable*, pages 3–23, 2007.

[20] D. Kwiatkowska. Surface growth at the reproductive shoot apex of Arabidopsis thaliana pin-formed 1 and wild type. *Journal of Experimental Botany*, 55(399):1021–1032, 2004.

[21] F. Labelle and J. R. Shewchuk. Anisotropic voronoi diagrams and guaranteed-quality anisotropic mesh generation. In *Proceedings of the Nineteenth Annual Symposium on Computational Geometry*, SCG '03, pages 191–200, 2003.

[22] B. Lévy and Y. Liu. Lp Centroidal Voronoi Tesselation and its applications. *ACM Transactions on Graphics*, 29(4), 2010.

[23] D. G. Lowe. Distinctive image features from scale-invariant keypoints. *International Journal of Computer Vision*, 60:91–110, 2004.

[24] M. K. Misztal, J. A. Brentzen, F. Anton, and K. Erleben. Tetrahedral mesh improvement using multi-face retriangulation. In *Proceedings of the 18th International Meshing Roundtable*, pages 539–555, 2009.

[25] B. Shapiro, H. Jönsson, P. Sahlin, M. Heisler, A. Roeder, M. Burl, E. Meyerowitz, and E. Mjolsness. Tessellations and Pattern Formation in Plant Growth and Development. In R. Van de Weijgaert, G. Vegter, J. Ritzerveld, and V. Icke, editors, *Tessellations in the Sciences: Virtues, Techniques and Applications of Geometric Tilings*. Springer-Verlag, 2008.

[26] B. E. Shapiro, C. Tobin, E. Mjolsness, and E. M. Meyerowitz. Analysis of cell division patterns in the arabidopsis shoot apical meristem. *Proceedings of the National Academy of Sciences*, 112(15):4815–4820, 2015.

[27] J. R. Shewchuk. Tetrahedral mesh generation by Delaunay refinement. In *Proceedings of the Symposium on Computational Geometry*, SCG '98, pages 86–95, 1998.

[28] J. R. Shewchuk. Two discrete optimization algorithms for the topological improvement of tetrahedral meshes. In *Unpublished manuscript*, 2002.

[29] G. Taubin. Curve and surface smoothing without shrinkage. In *Proceedings of the Fifth International Conference on Computer Vision (ICCV'95)*, pages 852–857, 1995.